

Disappearance of the polyelectrolyte peak in salt-free solutionsAlexandros Chremos^{✉*} and Ferenc Horkay*Section on Quantitative Imaging and Tissue Sciences, Eunice Kennedy Shriver National Institute of Child Health and Human Development, National Institutes of Health, Bethesda, Maryland 20892, USA*

(Received 12 March 2020; accepted 10 July 2020; published 27 July 2020)

We investigate the nature of the polyelectrolyte peak in salt-free solutions by molecular dynamics simulations using a minimal model of polyelectrolyte solutions that includes an explicit solvent and counterions and small angle scattering experiments. It is found that the polyelectrolyte peak progressively disappears as the strength of solvation for the charged species is increased and the scattering profiles start to resemble those of neutral polymer solutions. The disappearance of the polyelectrolyte peak coincides with the emergence of attractive interchain interactions over a wide range of length scales. These findings provide insights into the microscopic origin of the polyelectrolyte peak.

DOI: [10.1103/PhysRevE.102.012611](https://doi.org/10.1103/PhysRevE.102.012611)**I. INTRODUCTION**

Polyelectrolytes are charged macromolecules with unique solvating properties that are crucial to their biological function, such as DNA and proteins, which makes them essential for the development of many modern materials [1]. A characteristic feature of polyelectrolyte solutions is a broad peak in the scattering profiles observed by small angle neutron (SANS) and small angle x-ray (SAXS) studies, suggesting a liquidlike ordering on a length scale of the size of the polymers [2,3]. It is often referred to as the “polyelectrolyte peak” due to its ubiquitous nature, and its absence in neutral polymer solutions [4] has motivated extensive theoretical and experimental investigations to rationalize the peak’s behavior [3,5–15]. For example, the polyelectrolyte peak broadens and moves to higher wave vectors as the polyelectrolyte concentration is increased, suggesting that the liquidlike order diminishes as the polymer concentration is increased [16,17]. The peak also disappears by adding salt due to the screening of electrostatic interactions [10,17]. However, researchers have reported SANS and SAXS measurements indicating that several salt-free polyelectrolyte solutions, such as hyaluronate [18,19] and polyaspartic acid [20], do not exhibit a polyelectrolyte peak, suggesting that this scattering feature is *not* universal in polyelectrolyte solutions. The disappearance of the polyelectrolyte peak in salt-free conditions poses a significant challenge in establishing a general microscopic theory for polyelectrolyte solutions, as it is inherently linked to the following unresolved question [11]. *What is the microscopic origin of the polyelectrolyte peak?*

The challenge in establishing general microscopic models and theories for polyelectrolyte solutions lies in the complexity of these systems. Polyelectrolytes release a significant fraction of their counterions into polar solvents and this ionization process results in long-range repulsive Coulomb interactions between the polymer segments that cause the

polymer to swell [21]. While a fraction of the counterions is transiently bound to the polyelectrolyte chains, many of the solvated counterions form a diffuse ionic “cloud” around the chain due to residual unscreened polyelectrolyte charge with a constant dynamic exchange of counterions between bounded and unbounded states [22–24]. The importance of these unbound counterions has been advocated by Langmuir [25], Feynman *et al.* [26], and Ise and coworkers [27,28], as mediators of effective attractive interactions between like-charged particles. However, the influence of the ionic cloud on the structure of polyelectrolyte and particle solutions is not fully understood.

Recent molecular dynamics (MD) simulations [29,30] showed that the strength of solvation enhances the localization of the solvated charged species, e.g., the counterions within the ionic cloud, giving rise to effective interchain attractive interactions at different length scales depending on the type of solvation. These interactions operate on length scales on the order of the polymer size (long ranged) and polymer segment size (short ranged) for enhanced counterion solvation [29] and enhanced polyelectrolyte solvation [30], respectively. Here, we investigate how the structure of salt-free polyelectrolyte solutions is influenced by variation of *both* counterion and polyelectrolyte solvations, and we use SANS to validate the disappearance of the polyelectrolyte peak. Our findings reveal that the polyelectrolyte peak disappears when *both* long- and short-range attractive interchain interactions emerge in salt-free polyelectrolyte solutions.

II. METHODS AND MODELS**A. Experimental methods**

SANS measurements were made on the 10-m Small Angle Neutron Scattering instrument at National Institute of Standards and Technology on samples of chondroitin sulfate and hyaluronic acid in salt-free polyelectrolyte solutions, using wavelength $\lambda = 8 \text{ \AA}$, with wavelength spread $\Delta\lambda/\lambda = 0.13$. Two sample-detector distances were used, 4 and 10 m,

*alexandros.chremos@nih.gov

corresponding to an explored wave vector range $0.003 \text{ \AA}^{-1} < q < 0.2 \text{ \AA}^{-1}$ where $q = 4\pi/\lambda \sin(\theta/2)$, with θ being the scattering angle. The sample temperature during the experiment was maintained at $25 \pm 0.1 \text{ }^\circ\text{C}$. After radial averaging, corrections for incoherent background, detector response, and cell window scattering were applied. The neutron-scattering intensities were calibrated using water [31]. The molecular weights were $1.2 \times 10^6 \text{ Da}$ for hyaluronic acid and $40\,000 \text{ Da}$ for chondroitin sulfate. The polymer concentration in each system was 4% (m/m), corresponding to the semidilute concentration regime.

B. Simulation model

We employ a bead-spring model of Lennard-Jones (LJ) segments with charges bound by stiff harmonic bonds suspended in explicit LJ solvent particles, some of which are charged to represent counterions [23,24,32]; the particular model accounts for the short-ranged interactions of solvent needed to address ion and polymer solvation, while at the fixed time it enables long time and relatively large scale simulations that are required to study the associative behavior of polyelectrolyte solutions. All particles are assigned the same mass m , size σ , and strength of interaction ε . We set ε and σ as the units of energy and length; the cutoff distance for the LJ interaction potential is $r_c = 2.5 \sigma$. The size and energy parameters between i and j particles are set as $\sigma_{ii} = \sigma_{jj} = \sigma_{ij} = \sigma$ and $\varepsilon_{ii} = \varepsilon_{jj} = \varepsilon_{ij} = \varepsilon$, except for two energy interaction parameters: the first interaction parameter is between the solvent particles and the counterions ε_{CS} and the second interaction parameter is between the solvent particles and the polyelectrolyte segments ε_{PS} . All charged particles interact via the Coulomb potential (with a cutoff distance 10σ) and a relatively short-range Lennard-Jones potential of strength ε , and the particle-particle particle-mesh method is used [33].

The system is composed of a total of $N_t = 256\,000$ particles in a periodic cube of side L and volume V . The system includes $N_p = 100$ polyelectrolyte chains composed of $N = 41$ segments, each segment carrying a negative elementary charge $-e$, and $N_+ = N_p N$ monovalent counterions to satisfy electroneutrality. The number of neutral solvent particles is $N_0 = N_t - N_+ - N_p N$. The bonds between polymer segments are connected via a stiff harmonic spring, $V_H(r) = k(r - l_0)^2$, where $l_0 = \sigma$ is the equilibrium length of the spring, and $k = 1\,000 \varepsilon/\sigma^2$ is the spring constant. The Bjerrum length was set equal to $l_B = e^2/(\varepsilon_s k_B T) = 2.4 \sigma$, where T is the temperature, k_B is Boltzmann's constant, and ε_s is the dielectric constant of the medium. The systems were equilibrated at constant pressure $\langle P \rangle \approx 0.02$ and constant temperature $k_B T/\varepsilon = 0.75$ conditions, maintained by a Nosé-Hoover thermostat. Typical simulations equilibrate for $5\,000 \tau$ and data are accumulated over a $150\,000 \tau$ interval, where $\tau = \sigma(m/\varepsilon)^{1/2}$ is the MD time unit; the time step used was $\Delta t/\tau = 0.005$.

C. Calculation of the structure factor

To probe the structure of polyelectrolytes in solution, we focus on calculating the spatial correlations between the polymer segments. The structure factor, $S(q)$, is a suitable property for this purpose and describes the mean correlations in the

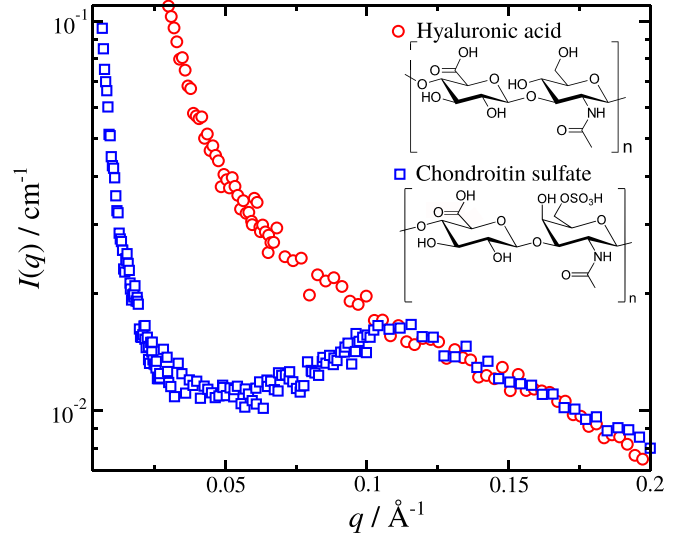


FIG. 1. Small angle neutron scattering profiles of chondroitin sulfate and hyaluronic acid in salt-free solutions and sodium (Na^+) counterions. The polymer concentration in each system was 4% (m/m).

positions of a collection of point particles distributed in space, and $S(q)$ is defined as

$$S(q) = \frac{1}{N_s} \left\langle \sum_{j=1}^{N_s} \sum_{k=1}^{N_s} \exp[-i\mathbf{q} \cdot (\mathbf{r}_j - \mathbf{r}_k)] \right\rangle \\ = \frac{1}{N_s} \left\langle \left(\sum_{j=1}^{N_s} \cos \mathbf{q} \cdot \mathbf{r}_j \right)^2 + \left(\sum_{j=1}^{N_s} \sin \mathbf{q} \cdot \mathbf{r}_j \right)^2 \right\rangle, \quad (1)$$

where $i = \sqrt{-1}$, $q = |\mathbf{q}|$ is the wave number, \mathbf{r}_j is the position of segment j , $\langle \rangle$ denote the time average, and N_s is the total number of polymer segments defined as $N_s = N_p M_w$.

III. RESULTS AND DISCUSSION

We produced SANS scattering profiles for chondroitin sulfate (ChS) and hyaluronic acid (HA) in salt-free solutions with sodium (Na^+) counterions (see Fig. 1). Both polymers play an important role in providing osmotic swelling pressure necessary for cartilage to act as a shock absorber [34]. Scattering profiles for both polymers in the semidilute regime have two common features.

(i) The scattering intensity scales as $I(q) \sim 1/q$ at the high- q regime, indicating that the scattering elements are rodlike as expected for individual polyelectrolyte conformations.

(ii) In the low- q regime, $I(q)$ exhibits a sharp upturn due to the formation of multichain structures commonly observed in associating liquids [35] and in polyelectrolyte solutions [14,36].

Despite the strong similarities in the monomer structure of these polyelectrolytes, polymer concentration, and electrostatic conditions, one system exhibits a well-defined scattering peak at intermediate length scales while the other does not (Fig. 1), in quantitative agreement with previous scattering studies [18–20]. However, this effect is not anticipated

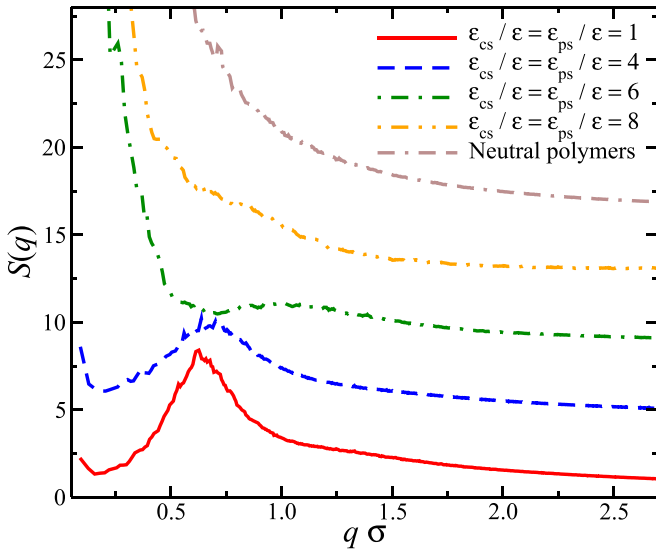


FIG. 2. Structure factor, $S(q)$, of salt-free polyelectrolyte solutions and neutral polymer solutions at the same polymer concentration obtained from molecular simulations. The curves are separated by four points along the y axis for clarity.

theoretically or by models based on the primitive model of polyelectrolyte solutions [5,6,21].

To probe the disappearance of the polyelectrolyte peak, we conducted MD simulations of an explicit solvent bead-spring model of polyelectrolyte solutions [23,24,32]. While the particular model is an extension of the primitive model of polyelectrolyte solutions [21,37], it differs by treating the

solvent *explicitly*, e.g., we can vary the strength of dispersion interactions between the solvent particles and the counterions ϵ_{CS} and between the solvent particles and the polyelectrolyte segments ϵ_{PS} with respect to the strength of solvent-solvent interactions ϵ . The scattering profiles are estimated by calculating the static structure factor $S(q)$ at the same polymer concentration and electrostatic conditions with variation of ϵ_{CS} and ϵ_{PS} . To better understand the underlying mechanism of these changes in $S(q)$, we utilize the potential of mean force of the segmental interchain interactions, $U(r)$, to map the structures found at different solvating conditions. We find that variation of ϵ_{CS} and ϵ_{PS} plays a crucial role in the form of $S(q)$ (Fig. 2) and $U(r)$ (Fig. 3), resulting in five distinct regimes.

Long-range repulsive interactions are the main characteristic features in $U(r)$ for solvents having weak solvation for both the counterions and the polyelectrolyte segments ($\epsilon_{CS}/\epsilon \lesssim \epsilon_{PS}/\epsilon \lesssim 5$) [see Fig. 3(a)]. This suggests that the effective interchain interactions can be described as N -valent charged points interacting with each other as $\frac{1}{r} \exp(-r)$ in the dilute regime, an approximation often used in the modeling of polyelectrolyte solutions [38]. The resulting $S(q)$ exhibits a scattering peak at length scales (q_p) on the order of the radius of gyration, $R_g \approx 2\pi/q_p$, along with a small or no upturn in the low- q regime indicative of a homogeneous polymer solution (Fig. 2). Greater suppression of the upturn is achieved by weaker solvation ($\epsilon_{CS}/\epsilon \approx \epsilon_{PS}/\epsilon \lesssim 1$), thus matching with the structures obtained from the primitive model of polyelectrolyte solutions [21,37] [see Fig. 3(b)]. In other words, a homogeneous polyelectrolyte solution occurs when the polyelectrolyte chains maximize their distance from

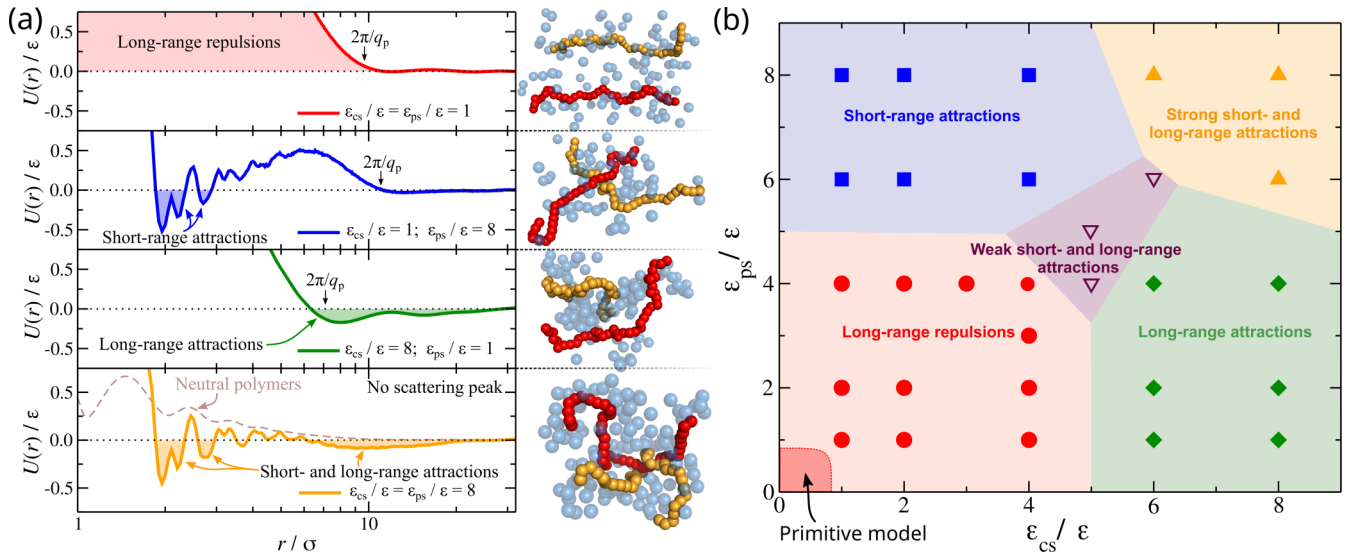


FIG. 3. (a) Potential of mean force, $U(r)$, based on the segmental intermolecular pair correlation $U(r) = -\ln[g(r)]$, as a function of the distance. The continuous and dashed lines correspond to polyelectrolyte and neutral polymer solutions. The highlighted regions outline $U(r)$ characteristic features. The downward pointed black arrows indicate the average position of the polyelectrolyte peak, q_p , found in $S(q)$. Screenshots of typical conformations of a pair of neighboring polyelectrolyte chains (in red and orange colors) for each case $U(r)$; counterions are transparent in blue color; solvent particles are rendered invisible for visualization purposes. (b) Morphology diagram of salt-free polyelectrolyte solutions as a function of the strength of solvation for the charged species. The highlighted regions and symbols approximately outline the boundaries between the different types of structures based on the resulting $U(r)$ of salt-free polyelectrolyte solutions. We also outline the region corresponding to structures resembling structures generated by the primitive model of polyelectrolyte solutions (see Ref. [29]).

each other, due to the interchain repulsive interactions driven by weak solvation.

When one type of solvation becomes stronger than the other, then more interfacial counterions dissolve in the solvent, leading to nearly complete ionization of the polymers [29,39]. Enhanced counterion solvation ($\epsilon_{CS}/\epsilon \gtrsim 5$ and $\epsilon_{PS}/\epsilon \lesssim 5$) gives rise to effective *long-range* interchain attractive interactions due to localization of counterions in ion-rich domains that bring polyelectrolyte chains closer together by wrapping around these counterion-rich domains [29]. On the other hand, enhanced polyelectrolyte solvation ($\epsilon_{CS}/\epsilon \lesssim 5$ and $\epsilon_{PS}/\epsilon \gtrsim 5$) increases the difference in mobility between the charged species, inducing depletionlike interactions that bring polyelectrolyte chains in close proximity to each other to form a polymer network; this effect gives rise to *short-range* attractive interactions in $U(r)$ [30] [see Fig. 3(a)]. The emergence of effective interchain attractive interactions reduces the homogeneity of the polyelectrolyte solution, which is reflected in $S(q)$ by a sharp upturn in the low- q regime [29,30], and provides support to experimental and theoretical observations of heterogeneous multichain structure formation [14,15,36,40]. All types of solvation discussed so far exhibit a well-defined peak in $S(q)$, and its position coincides with $U(r) \rightarrow 0$ at the length scales of the polymer size, $r \approx R_g \approx 2\pi/q_p$ [Fig. 3(a)], suggesting that q_p is associated with the characteristic length scale of interchain repulsive interactions in agreement with experimental observations [41]. Typical examples of $S(q)$ for the above mentioned cases are presented in previous work [29,30].

Now that we have an understanding of the structure of salt-free polyelectrolyte solutions that exhibit strong solvation on one of the charged species, we examine changes in $S(q)$ as the strength of solvation progressively increases for *both* counterions and polyelectrolyte segments by the same amount ($\epsilon_{CS} = \epsilon_{PS}$). We find that the peak in $S(q)$ becomes less pronounced, followed by a sharp upturn in the low- q regime. When the solvation becomes strong enough ($\epsilon_{CS}/\epsilon = \epsilon_{PS}/\epsilon \gtrsim 6$), then the peak in $S(q)$ disappears (see Fig. 2). Despite the resemblance in the scattering profiles of neutral polymer solutions, there are significant differences in $U(r)$. In neutral polymer solutions, $U(r)$ is dominated by an effective “soft” interchain repulsive interaction, which is entropic in origin [42], on the length scales of the polymer size [see Fig. 3(a)]. In polyelectrolyte solutions, $U(r)$ is dominated by the same-charge Coulomb interactions between the polymer segments, giving rise to steep repulsive interactions on length scales of the polymer size. Enhanced solvation for one of the charged species does not fully reduce these repulsive interactions, as discussed above. However, enhanced solvation for *both* charged species results in the emergence of *both* short- and long-range attractive interactions that effectively suppresses any long-ranged repulsions in $U(r)$ [Fig. 3(a)]. This effect greatly increases the probability of finding polyelectrolyte chains in close proximity with each other by forming meshlike structures due to short-range attractions, and large heterogeneous multichain structures resulting from long-ranged attractive interactions. These dynamic multichain structures are stable due to a significant localization of counterions near the center of mass of polyelectrolyte chains (Fig. 4). Another consequence of localization is the enhancement of

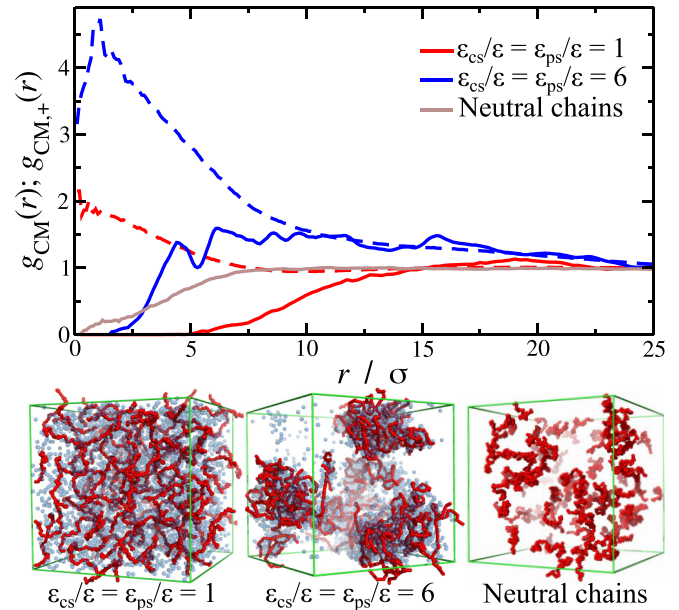


FIG. 4. Pair correlation function of the center of mass of polyelectrolyte chains $g_{CM}(r)$ (continuous lines) and the pair correlation function between the counterions around the center of mass of polyelectrolyte chains $g_{CM,+}(r)$ (dashed lines). Screenshots of polyelectrolyte solutions at different types of solvation are also presented; polyelectrolyte segments are in red; counterions are transparent in blue color; solvent particles are rendered invisible for visualization purposes. Results for neutral polymer solutions are also presented.

structure near the polyelectrolyte chains, resulting in small oscillatorylike peaks in the correlations of the solvated species seen in Fig. 3(a).

The formation of meshlike structures by like-charged polymer chains *without* exhibiting a characteristic length scale is not anticipated by contemporary theories and models of polyelectrolyte solutions, but it is consistent with experimental observations. It has been argued, based on the SANS scattering profiles, that HA chains form meshlike structures, which is further supported by deviations from ideal Newtonian behavior that depend on concentration and salt content observed in viscoelastic measurements [43]. The underlying mechanism that leads to such structures is assumed to be intermolecular associations, specifically hydrogen bonds [19]. However, this assumption fails to explain why the SANS responses of two polymers having similar monomer structures are different. Our findings suggest that the disappearance of the polyelectrolyte peak occurs at a balance of competitive interactions between the solvent particles and the charged species that lead to the emergence of effective short- and long-ranged attractions. Without this balance, the emergence of this scattering feature is expected to emerge as discussed above.

Different values of ϵ_{CS} correspond to different types of ions based on their enthalpy of solvation [44,45], e.g., $\epsilon_{CS}/\epsilon = 0.85, 1.25,$ and 1.6 in electrolyte solutions (no polymer chains) at low salt concentration $c < 0.5$ M for caesium, sodium, and lithium, respectively. Divalent ions are expected to exhibit values in the range $\epsilon_{CS}/\epsilon \sim 4$ to 7 in low salt

electrolyte solutions. However, we anticipate these values to change (i) in close proximity to polyelectrolyte chains where the dielectric permittivity decreases significantly (by a factor of 5 to 8) [46], (ii) when the packing of water molecules is disturbed by the polymer (both the degree of localization and orientational interactions such as hydrogen bonds, etc.), and (iii) in regions having high concentration of ions near the proximity of the polyelectrolyte chains (equivalent to the high salt limit). While these effects are not incorporated directly in our model, limitations inherited by the primitive model, their effects in a coarse-grained fashion are captured by the increased value in ϵ_{CS} and ϵ_{PS} , leading to the distribution of the charged species as seen in Fig. 4. This means that minor differences in the chemical structure between HA and ChS have the potential to influence both the ion-solvent and solvent-polymer interactions. Indeed, water molecules interact less strongly with the sulfate group compared with the pyranose ring [47], meaning that ϵ_{PS} is higher in HA than in ChS solutions. Moreover, the packing of water molecules and spatial dependence of dielectric permittivity in close proximity to polyelectrolyte chains are anticipated to be different, affecting the value of ϵ_{CS} even though counterions are the same in HA and ChS solutions. Taking these effects into consideration suggests that the differences in ϵ_{CS} and ϵ_{PS} between the HA and ChS solutions are significant enough to jump from one structural regime to another [Fig. 3(b)] as it is evident from the SANS data in Fig. 1.

IV. CONCLUSIONS

Our simulation results provide the basis for understanding the disappearance of the polyelectrolyte peak in salt-free conditions and provide an interpretation on why the scattering responses of two polyelectrolytes having similar monomer structures (hyaluronic acid and chondroitin sulfate)

are different: one exhibits a well-defined scattering peak while the other does not. In particular, our simulation of a coarse-grained polyelectrolyte model with an explicit solvent and counterions indicates that the polyelectrolyte peak becomes less pronounced along with a steep upturn in the low- q regime as the strength of solvation for both counterions and polyelectrolyte segments becomes progressively stronger. Eventually, the scattering peak disappears and the scattering profile resembles the profiles obtained for neutral polymer solutions. Unlike neutral polymer solutions, the disappearance of the polyelectrolyte peak is due to the emergence of effective interchain attractive interactions that are *both* short and long ranged. Long-ranged attractive interactions, induced by enhanced counterion solvation, lead to formation of heterogeneous multichain structures. Within these multichain structures, polyelectrolyte chains associate with each other at short distances, forming a polymer network or mesh due to enhanced polyelectrolyte solvation. Thus, the disappearance of the polyelectrolyte peak means that there is no characteristic length scale associated with the average distance between the polyelectrolyte chains. Our observations provide insights into the microscopic origin of the polyelectrolyte peak and reinforce the idea that solvent interactions with charged species are just as important as Coulomb interactions.

ACKNOWLEDGMENTS

This research was supported by the Intramural Research Program of the NICHD, NIH. We acknowledge the support of the National Institute of Standards and Technology, U.S. Department of Commerce, in providing the neutron research facilities used in this work. This work utilized facilities supported in part by the National Science Foundation under Grant No. DMR 0944772. The authors also thank J. F. Douglas and D. J. Audus for helpful discussions.

-
- [1] M. Muthukumar, *Macromolecules* **50**, 9528 (2017).
 - [2] S. Förster, M. Schmidt, and M. Antonietti, *Polymer* **31**, 781 (1990).
 - [3] F. Horkay and B. Hammouda, *Colloid Polym. Sci.* **286**, 611 (2008).
 - [4] P. J. Debye, *Phys. Colloid Chem.* **51**, 18 (1947).
 - [5] P. G. de Gennes, P. Pincus, and R. Velasco, *J. Phys. (Paris)* **37**, 1461 (1976).
 - [6] T. J. Odijk, *Macromolecules* **12**, 688 (1979).
 - [7] L. Wang and V. A. Bloomfield, *Macromolecules* **24**, 5791 (1991).
 - [8] W. Essafi, F. Lafuma, and C. E. Williams, *J. Phys. II France* **5**, 1269 (1995).
 - [9] J.-L. Barrat and F. Joanny, *Adv. Chem. Phys.* **94**, 1 (1996).
 - [10] B. D. Ermi and E. J. Amis, *Macromolecules* **30**, 6937 (1997).
 - [11] A. Yethiraj, *Phys. Rev. Lett.* **78**, 3789 (1997).
 - [12] A. Yethiraj, *J. Chem. Phys.* **108**, 1184 (1998).
 - [13] B. D. Ermi and E. J. Amis, *Macromolecules* **31**, 7378 (1998).
 - [14] Y. Zhang, J. F. Douglas, B. D. Ermi, and E. J. Amis, *J. Chem. Phys.* **114**, 3299 (2001).
 - [15] M. Muthukumar, *Polymer Science Series A* **58**, 852 (2016).
 - [16] A. Yethiraj and C.-Y. Shew, *Phys. Rev. Lett.* **77**, 3937 (1996).
 - [17] V. M. Prabhu, E. J. Amis, D. P. Bossev, and N. Rosov, *J. Chem. Phys.* **121**, 4424 (2004).
 - [18] M. Villetti, R. Borsali, O. Diat, V. Soldi, and K. Eukada, *Macromolecules* **33**, 9418 (2000).
 - [19] F. Horkay, P. J. Basser, D. J. Londono, A.-M. Hecht, and E. Geissler, *J. Chem. Phys.* **131**, 184902 (2009).
 - [20] F. Horkay, A. M. Hecht, and E. Geissler, *J. Polym. Sci. Pol. Phys.* **44**, 3679 (2006).
 - [21] M. J. Stevens and K. Kremer, *Phys. Rev. Lett.* **71**, 2228 (1993).
 - [22] D. Hinderberger, G. Jeschke, and H. W. Spiess, *Macromolecules* **35**, 9698 (2002).
 - [23] T. S. Lo, B. Khusid, and J. Koplik, *Phys. Rev. Lett.* **100**, 128301 (2008).
 - [24] A. Chremos and J. F. Douglas, *Soft Matter* **12**, 2932 (2016).
 - [25] I. Langmuir, *J. Chem. Phys.* **6**, 873 (1938).
 - [26] R. P. Feynman, R. B. Leighton, and M. Sands, *The Feynman Lecture on Physics* (Addison-Wesley, Reading, MA, 1963).
 - [27] I. Sogami and N. Ise, *J. Chem. Phys.* **81**, 6320 (1984).

- [28] N. Ise and H. Yoshida, *Acc. Chem. Res.* **29**, 3 (1996).
- [29] A. Chremos and J. F. Douglas, *J. Chem. Phys.* **147**, 241103 (2017).
- [30] A. Chremos and J. F. Douglas, *J. Chem. Phys.* **149**, 163305 (2018).
- [31] P. J. Lindner, *Appl. Cryst.* **33**, 807 (2000).
- [32] R. Chang and A. Yethiraj, *J. Chem. Phys.* **118**, 6634 (2003).
- [33] R. W. Hockney and J. W. Eastwood, *Computer Simulation Using Particles* (Taylor & Francis, London, 1989).
- [34] A. Maroudas and K. E. Kuettner, *Methods in Cartilage Research* (Academic, New York, 1990).
- [35] F. Sciortino, E. Bianchi, J. F. Douglas, and P. Tartaglia, *J. Chem. Phys.* **126**, 194903 (2007).
- [36] H. Matsuoka, D. Schwahn, and N. Ise, *Macromolecules* **24**, 4227 (1991).
- [37] M. J. Stevens and K. Kremer, *J. Chem. Phys.* **103**, 1669 (1995).
- [38] J. P. Hansen and H. Löwen, *Annu. Rev. Phys. Chem.* **51**, 209 (2000).
- [39] A. Chremos and J. F. Douglas, *Gels* **4**, 20 (2018).
- [40] M. Muthukumar, *Proc. Natl. Acad. Sci. USA* **113**, 12627 (2016).
- [41] C. E. Williams, M. Nierlich, J. P. Cotton, G. Jannink, F. Boue, M. Daoud, B. Farnoux, C. Picot, P. G. Degennes, M. Rinaudo *et al.*, *J. Polym. Science Polym. Lett. Ed.* **17**, 379 (1979).
- [42] P. J. Flory and W. R. Krigbaum, *J. Chem. Phys.* **18**, 1086 (1950).
- [43] E. Fouissac, M. Milas, and M. Rinaudo, *Macromolecules* **26**, 6945 (1993).
- [44] M. Andreev, A. Chremos, J. de Pablo, and J. F. Douglas, *J. Phys. Chem. B* **121**, 8195 (2017).
- [45] M. Andreev, J. de Pablo, A. Chremos, and J. F. Douglas, *J. Phys. Chem. B* **122**, 4029 (2018).
- [46] H. Gong, G. Hocky, and K. F. Freed, *Proc. Natl. Acad. Sci. USA* **105**, 11146 (2008).
- [47] R. Servaty, J. Schiller, H. Binder, and K. Arnold, *Int. J. Biol. Macromol.* **28**, 121 (2001).